Characterization of electro-optic coefficients r13 , r23 and r33 in single crystalline BaTiO3 thin films

Yu Cao, Nour Al Meselmene, El Hadj Dogheche, Ping Yang, Parikshit Moitra, Shi Qiang Li, Thirumalai Venkatesan, Aaron Danner

Research Article | Vol. 13, No. 1 / 1 Jan 2023 / Optical Materials Express 152
Optical Materials EXPRESS

Characterization of electro-optic coefficients r_{13}, r_{23} and r_{33} in single crystalline $BaTiO_3$ thin films

Yu Cao,[1] Nour Al Meselmene,[2] Elhadj Dogheche,[2] Ping Yang,[3] Parikshit Moitra,[4] Shi Qiang Li,[4] Thirumalai Venkatesan,[1,5] and Aaron Danner[1,*]

[1]Department of Electrical and Computer Engineering, National University of Singapore, 4 Engineering Drive 3, 117583, Singapore
[2]Université Polytechnique Hauts de France, Institut d'Electronique, de Microélectronique et de Nanotechnologie - site de Valenciennes, IEMN CNRS UMR 8520, Valenciennes, 59309, France
[3]Singapore Synchrotron Light Source (SSLS), National University of Singapore, 5 Research Link, 117603, Singapore
[4]Institute of Materials Research and Engineering, 2 Fusionopolis Way, Innovis, 138634, Singapore
[5]Center for Quantum Research and Technology, University of Oklahoma, Norman OK 73071, USA
*adanner@nus.edu.sg

Abstract: We report experimental characterization of DC electro-optic coefficients r_{13}, r_{23} and r_{33} in thin film single crystalline $BaTiO_3$ on $DyScO_3$. The epitaxial $BaTiO_3$ thin film is sandwiched between a $SrRuO_3$ bottom electrode and an indium tin oxide (ITO) top electrode. We characterize the DC electro-optic coefficients r_{13}, r_{23}, and r_{33} by the prism coupling method at 636.6 nm for the $BaTiO_3$ thin film. The results show the DC coefficients $r_{13} = 4.2$ pm/V, $r_{23} = 4.6$ pm/V and $r_{33} = 9.0$ pm/V.

1. Introduction

Barium titanate ($BaTiO_3$, or BTO) has excellent electro-optic properties, with its largest r-parameter (unclamped (stress-free) $r_{42} = 1300$ pm/V, clamped (strain-free) $r_{42} = 730$ pm/V) [1] more than an order of magnitude larger than that of traditional lithium niobate ($LiNbO_3$, $r_{33} = 30.9$ pm/V) [2–4], and the other terms of its Pockels matrix also have decent strength (unclamped $r_{13} = 8$ pm/V, $r_{33} = 105$ pm/V, clamped $r_{13} = 10.2$ pm/V, $r_{33} = 40.6$ pm/V) [1]. Thin film $BaTiO_3$ grown on a substrate of low refractive index has advantages over bulk $BaTiO_3$ in several aspects, such as better vertical optical confinement, structural stability, higher phase transition temperature, etc. [5–9]. Thin film $BaTiO_3$ on an MgO substrate has been explored in quite a few studies and has shown, though weaker than that of its bulk, as strong or even stronger electro-optic effects compared to lithium niobate [10–19]. Even though r_{42} or r_{51} are the largest parameters in the Pockels matrix and are more widely studied, the r values along the c-axis (or z-axis) of $BaTiO_3$ thin film are yet to be studied [20–22]. Despite r_{42} (or r_{51}) being large, there is a key utility difference between r_{42} (or r_{51}) and r_{13} (or r_{23}, r_{33}). The former are off-diagonal Pockels terms such that an applied voltage will induce off-diagonal terms of refractive index causing polarization rotation of any mode within the influence of the applied field, while the latter only induce changes in the diagonal terms of the permittivity matrix and thus maintain polarization, causing only phase slip [2]. To the best of our knowledge this is the first report of the r_{13} (or r_{23}, r_{33}) values in $BaTiO_3$ thin film. There has been an investigation of the vertical electro-optic effect in $BaTiO_3$ polycrystalline thin film on MgO [23], but due to the random distribution of the polarization (or c-axis direction) in each domain, the effect probed is actually an effective r-value in the vertical direction instead of the actual r_{13}, r_{23}, r_{33} values, whereas in our single crystalline $BaTiO_3$ thin film, these values can be disentangled. In this study we characterize the r_{13}, r_{23}, r_{33} parameters by measuring the effect of variable applied vertical DC electric fields on

#474245 https://doi.org/10.1364/OME.474245
Journal © 2023 Received 29 Aug 2022; revised 2 Dec 2022; accepted 3 Dec 2022; published 14 Dec 2022

Optical Materials EXPRESS

the refractive indices of propagating optical slab modes. Although the resulting values we found are much smaller than those of the off-diagonal terms typically reported, the utility value of a having polarization-maintaining controllable phase shift in device design is important which is why these terms should not be overlooked, as this ability is absent when using r_{42} or r_{51}.

We grow $BaTiO_3$ on a $DyScO_3$ (DSO) substrate with $SrRuO_3$ (SRO) and indium tin oxide (ITO) as the bottom and top electrodes, respectively, to characterize the vertical electro-optic coefficient (r_{13}, r_{23}, r_{33}) of the $BaTiO_3$ layer. $DyScO_3$ (110) has been used as the substrate for $BaTiO_3$ epitaxial growth due to the small lattice mismatch [24].

2. Experiments, results, and discussion

2.1. Prism coupling measurement and birefringent refractive indices of $DyScO_3$

To obtain refractive indices of $BaTiO_3$, we need to first characterize the refractive indices of the $DyScO_3$ substrate. $DyScO_3$ has an orthorhombic crystal structure (a≠b≠c), and is thus expected to be birefringent [24,25]. We measured the refractive indices of two samples – the $DyScO_3$ (001) and $DyScO_3$ (110) substrates (CrysTec GmbH) – by the prism coupling method (Metricon), as shown in Fig. 1(a). The crystal orientation of $DyScO_3$ (001) and $DyScO_3$ (110) are shown in Fig. 1(b), where during measurement of refractive indices, the prism (TiO_2 rutile, prism index = 2.8654) was rotated to specific angles to align with the desired axis, and the resultant measurements with different configurations and at different wavelengths are labeled A-F. Figure 1(c) illustrates the polarization of incident light during measurement of the samples. For the measurement of the $DyScO_3$ (001) substrate, the laser's transverse electric (TE) polarization was aligned with the crystal's x-axis (A, D) and y-axis (B, E) with the transverse magnetic (TM) polarization corresponding to the z direction. For the measurement of the $DyScO_3$ (110) substrate, the laser's TE polarization was aligned with the z-axis (C, F), with the TM mode naturally aligning with the xy plane near an angle of 45° to the x-axis (nearly 43.555° because a≠b). Both samples were measured at a wavelength of 636.6 nm and 1548.4 nm. The results are shown in Table 1. Clear birefringence can be observed, where at 636.6 nm, $n_x = 2.0851 \pm 0.0002$, $n_y = 2.0802 \pm 0.0002$, and $n_z = 2.0370 \pm 0.0002$ [23]; n_{xy} can be calculated from measurements A, B by

$$\frac{1}{n^2(\theta)} = \frac{\cos^2(\theta)}{n_x^2} + \frac{sin^2(\theta)}{n_y^2} \tag{1}$$

to be 2.0828, which matches that from measurement C for $DyScO_3$ (110) very well. At 1548.4 nm, $n_x = 2.0490 \pm 0.0002$, $n_y = 2.0440 \pm 0.0002$, $n_z = 2.0040 \pm 0.0002$, and n_{xy} is calculated from measurements D, E to be 2.0466, matching very well with measurement F.

Table 1. Refractive indices of (a) $DyScO_3$ (001) and (b) $DyScO_3$ (110) substrate by the prism coupling method. The polarization of the incident light is denoted after the sample label.

Sample	Label	Refractive indices (636.6 nm)		Label	Refractive indices (1548.4 nm)	
	A-TE	n_x	2.0851	D-TE	n_x	2.0490
$DyScO_3$	A-TM	n_z	2.0373	D-TM	n_z	2.0035
(001)	B-TE	n_y	2.0802	E-TE	n_y	2.0440
	B-TM	n_z	2.0367	E-TM	n_z	2.0035
$DyScO_3$	C-TE	n_z	2.0370	F-TE	n_z	2.0040
(110)	C-TM	n_{xy}	2.0830	F-TM	n_{xy}	2.0464

The small birefringence may play a role in the polarization of the propagating light modes. When considering the construction of a phase modulator, such as a Mach-Zehnder modulator,

Optical Materials EXPRESS

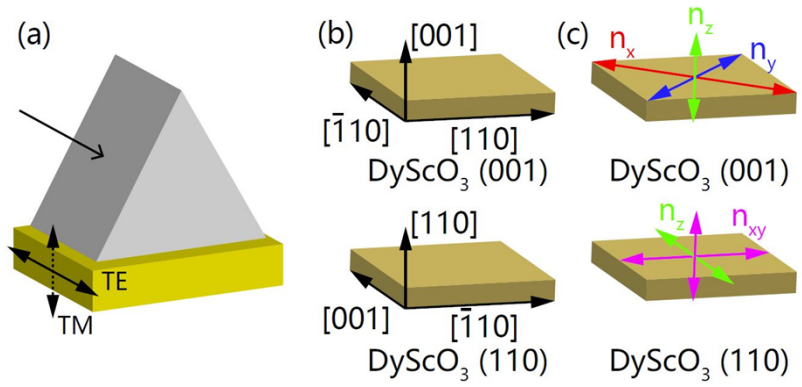

Fig. 1. (a) Schematic drawing of the prism coupling measurement setup. (b) Crystal structure and (c) refractive indices of $DyScO_3$ (001) and $DyScO_3$ (110). The crystal orientations are labeled in black, and the refractive indices are labeled in colors which correspond to the polarization directions in the prism coupling measurements.

this effect may be ignored as the amplitude change induced by the change of polarization is minor; on the other hand, for the design of a polarization modulator, it would possibly make a small difference. Therefore, in optical device design, a thick enough $BaTiO_3$ layer should be used to keep the confined optical field from overlapping the $DyScO_3$ substrate as much as possible, unless for some reason passive polarization rotation would be desirable. The results can be useful for further studies based on $BaTiO_3$ on $DyScO_3$.

2.2. *Electro-optic effect along the c-axis*

We then fabricated c-axis $BaTiO_3$ on a 100 mm^2 $DyScO_3$ (110) substrate with top and bottom electrodes, i.e., a structure of ITO/$BaTiO_3$/$SrRuO_3$/$DyScO_3$ device (labeled as IBSD) by pulsed laser deposition (KrF laser, 248 nm wavelength), where $SrRuO_3$ (SRO) is used as the bottom electrode in the stack while ITO acts as top electrode. First, SRO was grown at 600°C under 100 mTorr oxygen gas pressure with a laser pulse energy density of 2 J cm^{-2}. Then, a corner was covered by a shadow mask after the deposition of the bottom electrode, for the convenience of exposing the SRO surface for subsequent electrode connection. Following this, the BTO layer was grown at 650°C under 10 mTorr with a laser pulse energy density of 1.5 J cm^{-2}, followed by cooling at 100 Torr oxygen gas pressure. The ITO top electrode was then deposited at room temperature under 10 mTorr oxygen gas pressure with a laser pulse energy density of 2 J cm^{-2}. Silver paste (SP) was used to attach electrical leads to the top and bottom electrodes of each sample, at different corners. The device configuration is shown in Fig. 2. For this device (IBSD), the thicknesses of the ITO, BTO and SRO layers were 60 nm, 860 nm, 10 nm, respectively. The growth rate of each material is first measured and the thicknesses of the various layers are subsequently monitored by growth time. The growth rates for SRO and BTO are measured by reflection high-energy electron diffraction (RHEED), while the growth rate for ITO is determined by growing ITO with a shadow mask covering the substrate followed by measuring the step profile in atomic force microscopy (AFM).

We then performed structural characterization. The sample showed a smooth surface with a sub-nanometer root mean square (RMS) roughness, as shown in the atomic force microscopy image in Fig. 3(a). The crystallinity of IBSD was characterized by X-ray diffraction (XRD), as presented in Fig. 3(b) and 3(c) in comparison with a reference $BaTiO_3$ thin film directly grown on $DyScO_3$. In Fig. 3(b) the XRD 2θ-ω scan shows that the $BaTiO_3$ layer in both has only (001) and (002) peaks, indicating single crystallinity oriented with the c-axis out-of-plane. In

Optical Materials EXPRESS

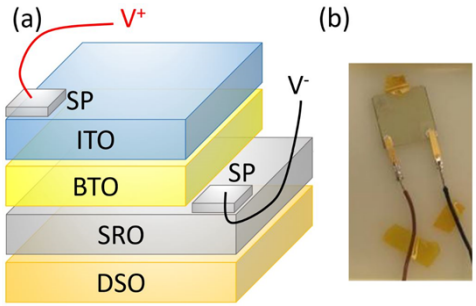

Fig. 2. (a) Schematic of the device structure and (b) picture of the actual device ITO/$BaTiO_3$/$SrRuO_3$/$DyScO_3$ (IBSD). SP refers to silver paste.

Fig. 3(c) compares the rocking curve of both at the $BaTiO_3$ (002) peak, where the full width at half maximum (FWHM) in IBSD is much larger than that of the reference $BaTiO_3$ thin film. This indicates that although the $BaTiO_3$ in the former is c-axis oriented, the c-axis alignment is not as good as with the latter. This degradation in crystal quality is due to the existence of the SRO buffer layer which affects subsequent $BaTiO_3$ growth.

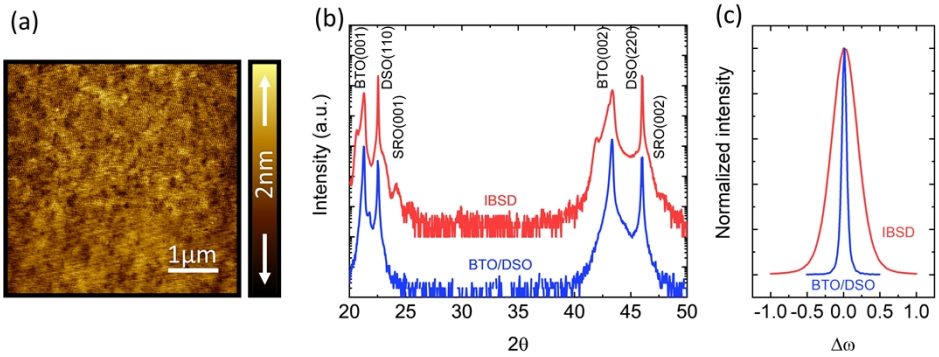

Fig. 3. Structural characterization of IBSD. (a) AFM surface topography of IBSD, with RMS roughness of 0.279 nm. (b) XRD 2θ-ω scan of IBSD (colored in red) showing a single crystalline c-axis oriented $BaTiO_3$ (BTO) thin film, in comparison with $BaTiO_3$ on $DyScO_3$ (colored in blue). (c) XRD rocking curve at the $BaTiO_3$ (002) peak of IBSD (colored in red), with the FWHM of 0.41°, in comparison with 0.07° for $BaTiO_3$ on $DyScO_3$ (colored in blue).

XRD reciprocal space mapping (RSM) is performed to investigate the strain state of the $BaTiO_3$ thin film in IBSD, as shown in Fig. 4. $BaTiO_3$ is strained and clamped to the substrate. The RSM is done near $BaTiO_3$ (002), (-103) and (013). In the RSM plots, H, K, L represent the reciprocal lattice indices constructed in reference to the reciprocal lattice constants of $DyScO_3$, where the horizontal axes H and K represent the in-plane reciprocal lattice, while vertical axis L represents the out-of-plane reciprocal lattice. (H and K represent the two orthogonal in-plane directions.) Fig. 4(a, b) show the RSM near $BaTiO_3$ (002) in the H and K directions, respectively, with the distribution in L illustrating the spreading in the out-of-plane reciprocal lattice, which corresponds to the lattice relaxation as shown in Fig. 4(c, d). Figure 4(c, d) shows the in-plane reciprocal lattices. The SRO (-103) and (013) peaks are aligned with those of the $DyScO_3$ substrates with the same H and K values, indicating that the thin layer of SRO is fully strained to the substrate. On the other hand, we can observe the $BaTiO_3$ (-103) and (013) peaks shifting

Optical Materials EXPRESS

from the substrate H and K values to smaller absolute H and K values, indicating in-plane strain relaxations in the two directions as the $BaTiO_3$ layer gets thicker.

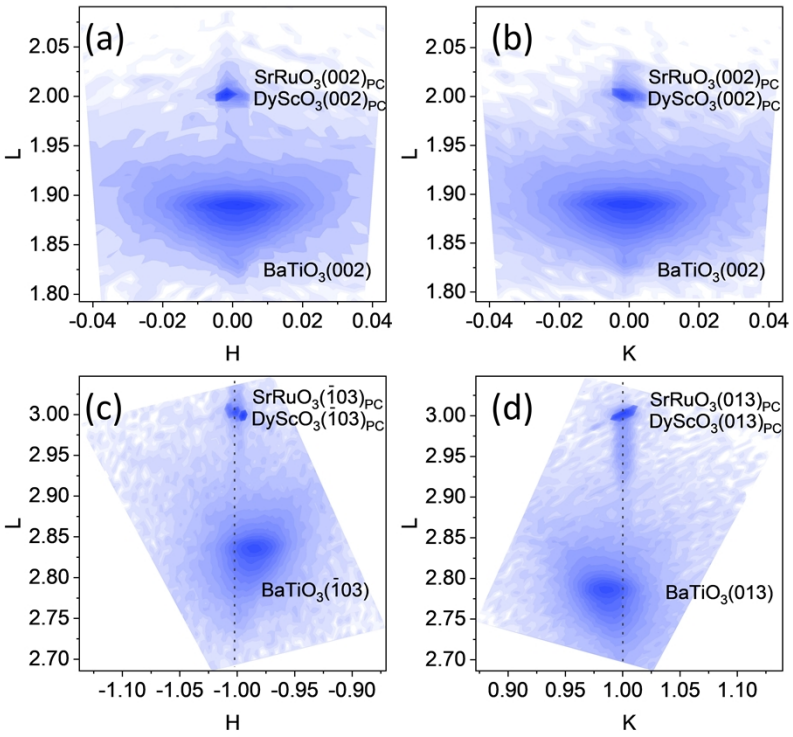

Fig. 4. XRD reciprocal space mapping (RSM) on IBSD near $BaTiO_3$ (002) (a, b), (-103) (c) and (013) (d). Horizontal axes H and K represent the in-plane reciprocal lattice, while vertical axis L represents the out-of-plane reciprocal lattice. H, K, L values are labeled in reference to the reciprocal lattice constants of $DyScO_3$. Pseudo cubic (PC) lattice index notations are used for $DyScO_3$ and $SrRuO_3$, respectively, in the figures for convenience of comparison. A bluer color corresponds to a higher intensity. The dashed lines in (c, d) represent the H and K values of the substrate as a guide to the eye.

The prism coupling method is used to characterize the refractive index, with a TE and TM polarized laser at a wavelength of 636.6 nm, as illustrated in Fig. 1(a). This wavelength is chosen because ITO is highly transparent at 636.6 nm and lossy at 1548.4 nm. The slab mode indices are first measured without an applied voltage, and then with applied voltages. The relationship between refractive index changes and applied electric field is

$$\Delta\varepsilon_{ij} = -\varepsilon_0 n_i^2 n_j^2 r_{lk} V_k \tag{2}$$

where $\Delta\varepsilon_{ij}$ is the square of the element (i, j) in the refractive index change matrix, n_i or n_j are the i^{th} or j^{th} respective elements of the diagonal terms of the refractive index tensor, r_{lk} the electro-optic coefficient in compressed index form and V_k the electric field in the k direction. Index changes induced by r_{13}, r_{23}, r_{33} are along the diagonal of the index tensor and hence do not alter polarization states if the propagating optical mode is aligned with one of the crystal's principal axes, which is the ordinary situation [2].

To distinguish the crystal orientation from that of $DyScO_3$, we use the $BaTiO_3$ crystal lattice axes a, b, c to describe the sample orientation. The IBSD sample was first positioned where the TE polarization was along the a direction, and then TE slab modes were measured, with

Optical Materials EXPRESS

results shown in Fig. 5(a); then the sample was rotated in-plane by 90 degrees to align the TE polarization with the b direction and the measurement was repeated with results shown in Fig. 5(b). The measured data are linearly fitted and electro-optic coefficients are calculated using Eq. (2) with the fitted slope. The results show that r_{13} and r_{23} values are not equal, due to the small in-plane anisotropy in $BaTiO_3$ mediated from $DyScO_3$ substrate, yet they show only a very small birefringence because of the partially relaxed state of $BaTiO_3$. Note that the measured coercive field is 496 kV/cm in the $BaTiO_3$ thin film, while the range of electric field applied in the r measurements (< 233 kV/cm) is smaller than the coercive field. In the experiment, we verified through repeated DC scans (i.e., when this procedure is altered) that no hysteresis in the refractive index vs. applied field was observed, consistent with there being little domain switching at these applied fields.

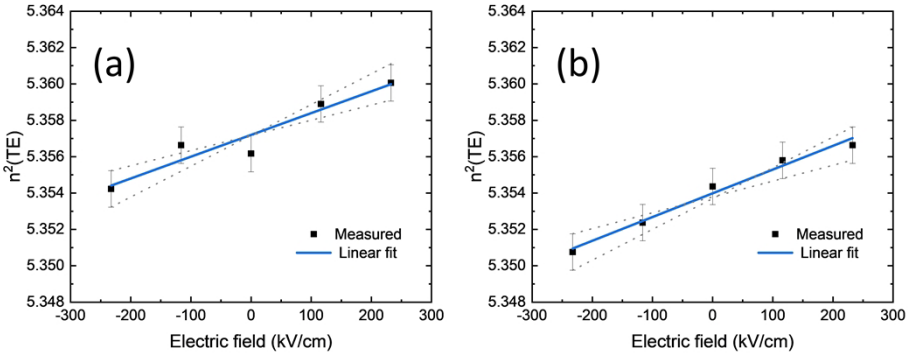

Fig. 5. DC electro-optic effect in ITO/BTO/SRO/DSO (IBSD) measured at 636.6 nm wavelength with the TE polarization aligned with the sample a-axis (a) and b-axis (b) direction. The slope of the linear fit for the measured data is used to calculate the electro-optic coefficients, where $r_{13} = 4.2 \pm 1.7$ pm/V and $r_{23} = 4.6 \pm 1.5$ pm/V. The error bars for each measurement of the square of the refractive index in the diagrams are inferred from known error of table position (i.e., angle error during prism coupling), and provide an evaluation of a maximum and minimum linear fitting slope (dashed lines) within the error bars. The slopes of the dotted lines are subsequently used to calculate the upper and lower bound errors for the r values. The larger error of the two is chosen to represent the error for the r values.

Then, incident laser light is set to TM, and TM slab modes are measured. Figure 6 shows the results and r_{33} is measured to be 9.0 ± 2.1 pm/V. The observed reduction of these r values as compared with the bulk values can be due to the degraded crystallinity, as compared above in Fig. 3. Despite the fact that the measured coefficients are smaller than what would be expected in a bulk crystal, it is known that bulk $BaTiO_3$ is comparatively limited in utility for device fabrication (the phase transition at 120 °C being severely limiting in terms of cleanroom processes, for instance) while this thin film $BaTiO_3$ grown on DSO more amenable to device fabrication due to excellent optical confinement, good thermal stability and a much higher phase transition temperature [9]. Therefore, potential device applications are still possible utilizing these somewhat lower coefficients. At this point, we have characterized all three r_{i3} values under an applied DC electric field.

To further understand the reduced r values and their relationship with crystallinity, we replace the SRO bottom electrode layer with another conducting layer $La_{0.67}Sr_{0.33}MnO_3$ (LSMO), which has a different lattice constant. LSMO has a larger lattice mismatch with the $DyScO_3$ substrate (1.96%), in comparison with that of SRO (0.7%). For such a device ITO/$BaTiO_3$/LSMO/$DyScO_3$ (labeled as IBLD), the thickness of the ITO, $BaTiO_3$ and LSMO layers were 60 nm, 700 nm, 6 nm, respectively. The LSMO layer is grown at 600°C under 100 mTorr oxygen gas pressure

Optical Materials EXPRESS

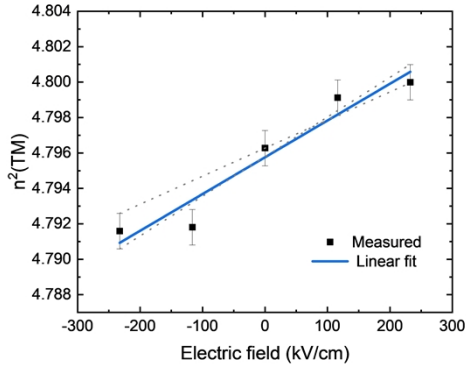

Fig. 6. DC electro-optic effect in ITO/BTO/SRO/DSO (IBSD) measured at 636.6 nm wavelength with TM polarization. The slope of the linear fit for the measured data is used to calculate the electro-optic coefficient $r_{33} = 9.0 \pm 2.1$ pm/V. Dashed lines represent the maximum and minimum slope for linear fitting within error bars, as described in the caption of Fig. 5.

with a laser pulse energy density of 2 J cm^{-2}, while growth for the other layers is the same. Like IBSD, the resulting device has a similar smooth surface, as shown in Fig. 7(a). But due to larger lattice mismatch, the BTO layer has a degraded crystal quality, presenting a major BTO (001) orientation with an impurity BTO (110) orientation, as shown in Fig. 7(b).

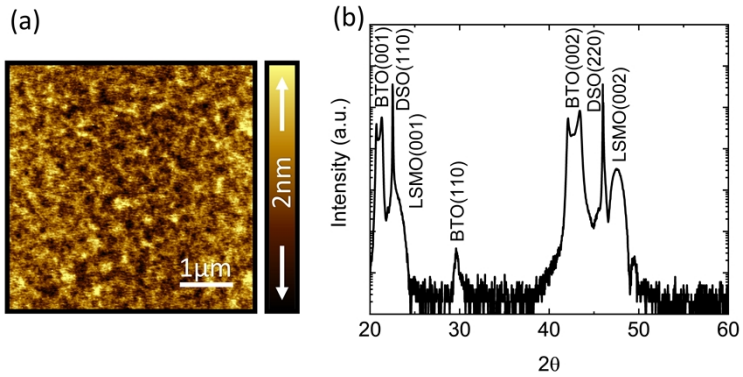

Fig. 7. Structural characterization of IBLD. (a) AFM surface topography of IBLD, with an RMS roughness of 0.389 nm. (b) XRD 2θ-ω scan of IBLD showing a major BTO (001) orientation with an impurity BTO (110) orientation.

Then, r_{13} and r_{33} are subsequently measured for IBLD using the same method described above for IBSD. Figure 8 shows the results. r_{13} and r_{33} were measured as 2.9 ± 1.5 pm/V and 5.8 ± 1.4 pm/V respectively, and these values are smaller than those of IBSD. This can be due to the existence of impurity phases in the $BaTiO_3$ layer. Comparing r values for IBSD and IBLD, we observe that the BTO layer with better crystallinity has a stronger DC electro-optic effect.

Optical Materials EXPRESS

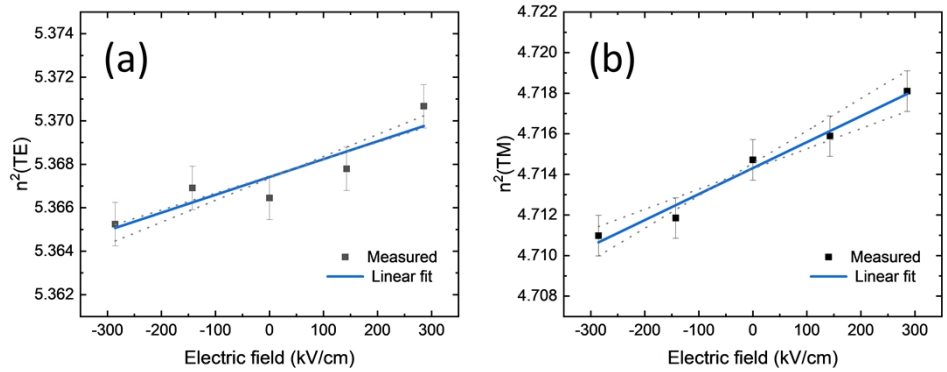

Fig. 8. DC electro-optic effect r_{13} (a) and r_{33} (b) in IBLD at 636.6 nm wavelength with TE polarization in line with sample a-axis direction. The coefficients r_{13} and r_{33} are measured 2.9 ± 1.5 pm/V and 5.8 ± 1.4 pm/V. Dashed lines represent the maximum and minimum slope for linear fitting within error bars, as described in the caption of Fig. 5.

3. Conclusion

In summary, we characterized the DC electro-optic coefficients r_{13}, r_{23} and r_{33} in single crystalline $BaTiO_3$ thin film with ITO and $SrRuO_3$ as top and bottom electrodes respectively by the prism coupling method. We first characterized the birefringent refractive indices of $DyScO_3$, with $n_x = 2.085$, $n_y = 2.080$, $n_z = 2.037$ at 636.6 nm wavelength and $n_x = 2.049$, $n_y = 2.044$, $n_z = 2.004$ at 1548.4 nm. We then characterized the DC electro-optic coefficients at 636.6 nm. A small difference is observed in r_{13} (4.2 pm/V) and r_{23} (4.6 pm/V) due to the small in-plane anisotropy in BTO thin film mediated from DSO substrate, yet are nearly isotropic in-plane because of the relaxed nature of the $BaTiO_3$ thin film. r_{33} is a bit larger (9.0 pm/V). These measured values are smaller than those of bulk values, and this can be attributed to the degraded crystallinity resulting from the insertion of the bottom electrode buffer layer during film growth. This is supported by a subsequent measurement of r values on another device IBLD where the $BaTiO_3$ has an impurity phase. If this hypothesis is false, on the other hand, then other, perhaps interesting, physical effects may be behind the observed relationship between crystal structure and electro-optic coefficient magnitude. Despite the fact that they are small, as discussed before, r_{13}, r_{23}, r_{33} can provide a particular functionality to device designs making use of the electro-optic effect in $BaTiO_3$ as they permit controllable polarization-maintaining phase shifts. Despite these values being small, they provide a clear demonstration of electro-optic modulation within thin film $BaTiO_3$, especially considering the good optical confinement and thermal stability of the $BaTiO_3$.

Funding. National Research Foundation Singapore (NRF-CRP24-2020-0003).

Acknowledgement. This work is supported by the Singapore National Research Foundation (NRF) under the Competitive Research Programs (CRP Grant No. NRF-CRP24-2020-0003). P.Y. is supported by SSLS via NUS Core Support C-380-003-003-001. The authors would also like to acknowledge the Singapore Synchrotron Light Source (SSLS) for providing the facilities necessary for conducting the research. The SSLS is a National Research Infrastructure under the National Research Foundation Singapore. This work is supported by the Université Polytechnique Hauts-de-France (UPHF) under the Competitive Research Programs (Grant no: AAP 15-2021). The authors would like to acknowledge the platform FUMAP at IEMN site Valenciennes for providing the facilities necessary for conducting the optical and electrooptical measurements.

Disclosures. The authors declare no conflicts of interest.

Data availability. Data underlying the results presented in this paper are not publicly available at this time but may be obtained from the authors upon reasonable request.

Optical Materials EXPRESS

References

1. M. Zgonik, P. Bernasconi, M. Duelli, R. Schlesser, P. Günter, M. H. Garrett, D. Rytz, Y. Zhu, and X. Wu, "Dielectric, elastic, piezoelectric, electro-optic, and elasto-optic tensors of $BaTiO_3$ crystals," Phys. Rev. B **50**(9), 5941–5949 (1994).
2. R. W. Boyd, "Chapter 11 - The Electrooptic and Photorefractive Effects," in *Nonlinear Optics (Fourth Edition)*, R. W. Boyd, ed. (Academic Press, 2020), pp. 495–522.
3. C. Wang, M. Zhang, X. Chen, M. Bertrand, A. Shams-Ansari, S. Chandrasekhar, P. Winzer, and M. Lončar, "Integrated lithium niobate electro-optic modulators operating at CMOS-compatible voltages," Nature **562**(7725), 101–104 (2018).
4. A. Guarino, G. Poberaj, D. Rezzonico, R. Degl'Innocenti, and P. Günter, "Electro–optically tunable microring resonators in lithium niobate," Nat. Photonics **1**(7), 407–410 (2007).
5. P. Tang, D. J. Towner, T. Hamano, A. L. Meier, and B. W. Wessels, "Electrooptic modulation up to 40 GHz in a barium titanate thin film waveguide modulator," Opt. Express **12**(24), 5962 (2004).
6. K. J. Choi, M. Biegalski, Y. L. Li, A. Sharan, J. Schubert, R. Uecker, P. Reiche, Y. B. Chen, X. Q. Pan, V. Gopalan, L.-Q. Chen, D. G. Schlom, and C. B. Eom, "Enhancement of ferroelectricity in strained $BaTiO_3$ thin films," Science **306**(5698), 1005–1009 (2004).
7. D. M. Gill, B. A. Block, C. W. Conrad, B. W. Wessels, and S. T. Ho, "Thin film channel waveguides fabricated in metalorganic chemical vapor deposition grown $BaTiO_3$ on MgO," Appl. Phys. Lett. **69**(20), 2968–2970 (1996).
8. A. R. Damodaran, E. Breckenfeld, Z. Chen, S. Lee, and L. W. Martin, "Enhancement of ferroelectric curie temperature in $BaTiO_3$ films via strain-induced defect dipole alignment," Adv. Mater. **26**(36), 6341–6347 (2014).
9. Y. Cao, S. L. Tan, E. J. H. Cheung, S. Y. Siew, C. Li, Y. Liu, C. S. Tang, M. Lal, G. Chen, K. Dogheche, P. Yang, S. Pennycook, A. T. S. Wee, S. Chua, E. Dogheche, T. Venkatesan, and A. Danner, "A barium titanate-on-oxide insulator optoelectronics platform," Adv. Mater. **33**(37), 2101128 (2021).
10. S. Abel, F. Eltes, J. E. Ortmann, A. Messner, P. Castera, T. Wagner, D. Urbonas, A. Rosa, A. M. Gutierrez, D. Tulli, P. Ma, B. Baeuerle, A. Josten, W. Heni, D. Caimi, L. Czornomaz, A. A. Demkov, J. Leuthold, P. Sanchis, and J. Fompeyrine, "Large Pockels effect in micro- and nanostructured barium titanate integrated on silicon," Nat. Mater. **18**(1), 42–47 (2019).
11. S. Abel, T. Stöferle, C. Marchiori, C. Rossel, M. D. Rossell, R. Erni, D. Caimi, M. Sousa, A. Chelnokov, B. J. Offrein, and J. Fompeyrine, "A strong electro-optically active lead-free ferroelectric integrated on silicon," Nat. Commun. **4**(1), 1671 (2013).
12. I.-D. Kim, Y. Avrahami, L. Socci, F. Lopez-Royo, and H. L. Tuller, "Ridge waveguide using highly oriented $BaTiO_3$ thin films for electro-optic application," J. Asian Ceram. Soc. **2**(3), 231–234 (2014).
13. D. H. Kim and H. S. Kwok, "Pulsed laser deposition of $BaTiO_3$ thin films and their optical properties," Appl. Phys. Lett. **67**(13), 1803–1805 (1995).
14. F. Eltes, D. Caimi, F. Fallegger, M. Sousa, E. O'Connor, M. D. Rossell, B. Offrein, J. Fompeyrine, and S. Abel, "Low-loss $BaTiO_3$ –Si waveguides for nonlinear integrated photonics," ACS Photonics **3**(9), 1698–1703 (2016).
15. P. Girouard, P. Chen, Y. K. Jeong, Z. Liu, S.-T. Ho, and B. W. Wessels, "$\chi(2)$ modulator With 40-GHz modulation utilizing $BaTiO_3$ photonic crystal waveguides," IEEE J. Quantum Electron. **53**(4), 1–10 (2017).
16. M. Luo and D. Sun, "Ultra-efficient modulation of $BaTiO_3$ crystal thin film waveguide with a two-dimensional optic-electric field matching scheme," J. Appl. Phys. **123**(3), 034503 (2018).
17. P. Tang, D. J. Towner, A. L. Meier, and B. W. Wessels, "Low-loss electrooptic $BaTiO_3$ thin film waveguide modulator," IEEE Photonics Technol. Lett. **16**(8), 1837–1839 (2004).
18. P. Tang, D. J. Towner, A. L. Meier, and B. W. Wessels, "Low-voltage, polarization-insensitive, electro-optic modulator based on a polydomain barium titanate thin film," Appl. Phys. Lett. **85**(20), 4615–4617 (2004).
19. P. Tang, A. L. Meier, D. J. Towner, and B. W. Wessels, "$BaTiO_3$ thin-film waveguide modulator with a low voltage–length product at near-infrared wavelengths of 0.98 and 1.55 mm," Opt. Lett. **30**(3), 254 (2005).
20. A. Petraru, J. Schubert, M. Schmid, and C. Buchal, "Ferroelectric $BaTiO_3$ thin-film optical waveguide modulators," Appl. Phys. Lett. **81**(8), 1375–1377 (2002).
21. C. Xiong, W. H. P. Pernice, J. H. Ngai, J. W. Reiner, D. Kumah, F. J. Walker, C. H. Ahn, and H. X. Tang, "Active Silicon Integrated Nanophotonics: Ferroelectric $BaTiO_3$ Devices," Nano Lett. **14**(3), 1419–1425 (2014).
22. D. M. Gill, C. W. Conrad, G. Ford, B. W. Wessels, and S. T. Ho, "Thin-film channel waveguide electro-optic modulator in epitaxial $BaTiO_3$," Appl. Phys. Lett. **71**(13), 1783–1785 (1997).
23. F. Leroy, A. Rousseau, S. Payan, E. Dogheche, D. Jenkins, D. Decoster, and M. Maglione, "Guided-wave electro-optic characterization of $BaTiO_3$ thin films using the prism coupling technique," Opt. Lett. **38**(7), 1037 (2013).
24. B. Veličkov, V. Kahlenberg, R. Bertram, and M. Bernhagen, "Crystal chemistry of $GdScO_3$, $DyScO_3$, $SmScO_3$ and $NdScO_3$," Z. Für Krist. **222**(9), 466–473 (2007).
25. M. D. Biegalski, J. H. Haeni, S. Trolier-McKinstry, D. G. Schlom, C. D. Brandle, and A. J. V. Graitis, "Thermal expansion of the new perovskite substrates $DyScO_3$ and $GdScO_3$," J. Mater. Res. **20**(4), 952–958 (2005).